PHYSICS

Quantum control of flying doughnut terahertz pulses

Kamalesh Jana[1]*, Yonghao Mi[1], Søren H. Møller[1], Dong Hyuk Ko[1], Shima Gholam-Mirzaei[1], Daryoush Abdollahpour[1,2], Shawn Sederberg[3], Paul B. Corkum[1]*

The ability to manipulate the multiple properties of light diversifies light-matter interaction and light-driven applications. Here, using quantum control, we introduce an approach that enables the amplitude, sign, and even configuration of the generated light fields to be manipulated in an all-optical manner. Following this approach, we demonstrate the generation of "flying doughnut" terahertz (THz) pulses. We show that the single-cycle THz pulse radiated from the dynamic ring current has an electric field structure that is azimuthally polarized and that the space- and time-resolved magnetic field has a strong, isolated longitudinal component. We apply the flying doughnut pulse for a spectroscopic measurement of the water vapor in ambient air. Pulses such as these will serve as unique probes for spectroscopy, imaging, telecommunications, and magnetic materials.

INTRODUCTION

Locally modifying the spatiotemporal character of light leads to intricate light beams that are often called "vector beams" or "structured light" (*1*, *2*). With structured light, we open the potential for harnessing the topological properties of light, and topology has applications in many research fields including optical tweezers, communications, particle control, ultrafast metrology, and super-resolution microscopy (*1*–*6*). Recent advances in optical technology have enabled fine control over the spatial and temporal structure of light, independently. Structuring multiple properties of light simultaneously leads to unique classes of light and new regimes of light-matter interaction. The technology required to generate such beams is virtually nonexistent. In 1996, Hellwarth and Nouchi (*7*) mathematically described a new light mode that is a single-cycle light pulse having toroidal topology, called "flying doughnut"(FD) pulses that are nonseparable in space and time and contain strong magnetic or electric field components along their propagation axis (*7*). Recently, there has been substantial interest in creating such space-time–coupled toroidal light modes (*8*, *9*) in the terahertz (THz) region, where single-cycle pulses have been available for decades (*10*).

Despite the impressive progress in ultrafast optics and beam shaping technology, generation of such spatiotemporal light modes remains challenging mainly due to their complex beam structure and our inability to sculpt the entire bandwidth of the pulses. A few approaches based on nanostructured metasurfaces have been used to generate spatiotemporally tailored THz pulses (*8*, *11*–*13*). However, active manipulation of the THz modes using conventional metasurfaces is not possible as most metasurfaces are static with fixed functionalities once fabricated. Also, the metasurfaces cannot withstand high pump intensity beyond their thermal damage threshold. Hence, there are limited opportunities for achieving substantially higher THz conversion efficiencies using metasurfaces.

Quantum control is an effective way to generate and control currents in semiconductors by exploiting quantum interference between pathways connecting the same initial and final states (*14*–*16*). In our previous experiments, we have demonstrated structured current

generation by applying spatially structured light pulses to quantum control (*17*–*20*). We have also shown that almost any kind of current patterns can be generated using a combination of a circularly polarized near-infrared pulse and a linearly polarized visible light pulse whose phase front has been structured by a spatial light modulator (*18*, *19*). Each transient current element acts as a subwavelength source of the THz field and a large collection of such transient current elements constitutes an active metasurface that radiates structured, single-cycle THz pulses. Hence, quantum control allows us to generate exotic light modes from a planar semiconductor substrate, bypassing the need for nanostructured materials.

Here, we demonstrate a clear link between the spatial structure of the bichromatic optical fields, the currents that they generate, and the spatial structure of the radiated single-cycle THz pulse. Specifically, we use azimuthally polarized bichromatic optical fields to drive a ring current in gallium arsenide (GaAs). In one part of the experiments, we measure the spatio-vectorial structure of these currents. In the other, we collect the radiated single-cycle THz pulse and map its spatiotemporal properties using electro-optic sampling (EOS). We show that the single-cycle THz pulse radiated from the dynamic ring current has an electric field structure that is azimuthally polarized and that the space- and time-resolved magnetic field has a strong, isolated longitudinal component, which could be of great utility for THz magnetic field spectroscopy. The measured pulse is an FD in THz frequency domain. The link between the incident optical fields, the injected currents, and the radiated FD THz pulse is illustrated conceptually in Fig. 1A. Here, we note how easily the current structure and the structure of the radiated single-cycle THz pulse can be modified to allow the electric and magnetic fields to interchange roles, simply by changing the mode of the incident optical fields.

Having generated a FD, we exploit the fact that our FD THz pulse is propagating through ambient air that contains water vapor. By performing measurements in different humidity levels, we illustrate how absorption features are mapped onto the spatiotemporal structure of an FD.

RESULTS

Currents were generated in a GaAs substrate under the excitation of two-color femtosecond laser pulses with characteristics that are described in Materials and Methods and using an optical setup

[1]Joint Attosecond Science Laboratory, University of Ottawa and National Research Council Canada, 25 Templeton Street, Ottawa, ON K1N 6N5, Canada. [2]Department of Physics, Institute for Advanced Studies in Basic Sciences (IASBS), Zanjan 45137-66731, Iran. [3]School of Engineering Science, Simon Fraser University, 8888 University Drive, Burnaby, BC, V5A 1S6, Canada.
*Corresponding author. Email: kjana@uottawa.ca (K.J.); pcorkum@uottawa.ca (P.B.C.)

sketched in fig. S1. The fundamental pulse has a wavelength of 1480 nm, and its second harmonic has a wavelength of 740 nm. They induce two-photon and single-photon transitions in GaAs, respectively. When we use linearly polarized Gaussian laser pulses, the generated current is uniform and parallel to the local field across the beam profile. Therefore, quantum control driven with two azimuthally polarized vector laser pulses creates a local current vector that is likewise aligned along the local electric fields and, consequently, in a ring structure. In other words, the electric field structure of the driving beams is transferred to the generated current distribution. The spatio-vectorial distribution of the current was measured using a square-apertured (25 μm) low-temperature GaAs detector (17). The measured current structures are presented in Fig. 1B and clearly resemble a ring current. Again, we note that changing the polarization of the incident optical fields would result in the injection of a radial current arrangement.

We numerically confirm that a dynamic ring current similar to the one presented in Fig. 1B can be a source for an FD THz pulse by performing finite-difference time-domain (FDTD) simulations. In these simulations, we use a dynamic ring current density as a source and record the spatiotemporal structure of the fields that it radiates.

The spatiotemporal structure of the simulated electric field is shown in Fig. 1C. The spatio-spectral structure of the electric fields (fig. S2) bears clear resemblance to that expected from an FD pulse (8, 9). Figure 1D shows the spatiotemporal structure of the simulated magnetic field, which is of subcycle duration and whose spatial maximum coincides with the electric field singularity.

Motivated by this prediction, we measure the emitted THz radiation by free-space EOS, as depicted in Fig. 2A. For the measurement, the generated THz radiation is collected, collimated, and refocused onto a 1-mm-thick zinc-telluride (ZnTe) crystal with a pair of THz lenses (Tsurupica material), as described in Materials and Methods. A synchronized second harmonic probe beam (740 nm) is used to sample the THz pulse.

An exemplary THz waveform is shown in fig. S3A. Figure S3B depicts the power spectral density corresponding to this waveform. We note that the full bandwidth of the THz pulse was not captured in our measurement, as the electro-optic response of the detection crystal (ZnTe) is very weak beyond 5 THz. The detected THz waveform as a function of the relative phase of the two-color field ($\Delta\varphi_{\omega,2\omega}$) is presented in Fig. 2B. The sinusoidal dependence of the THz peak field on the relative phase ($\Delta\varphi_{\omega,2\omega}$) confirms that the THz
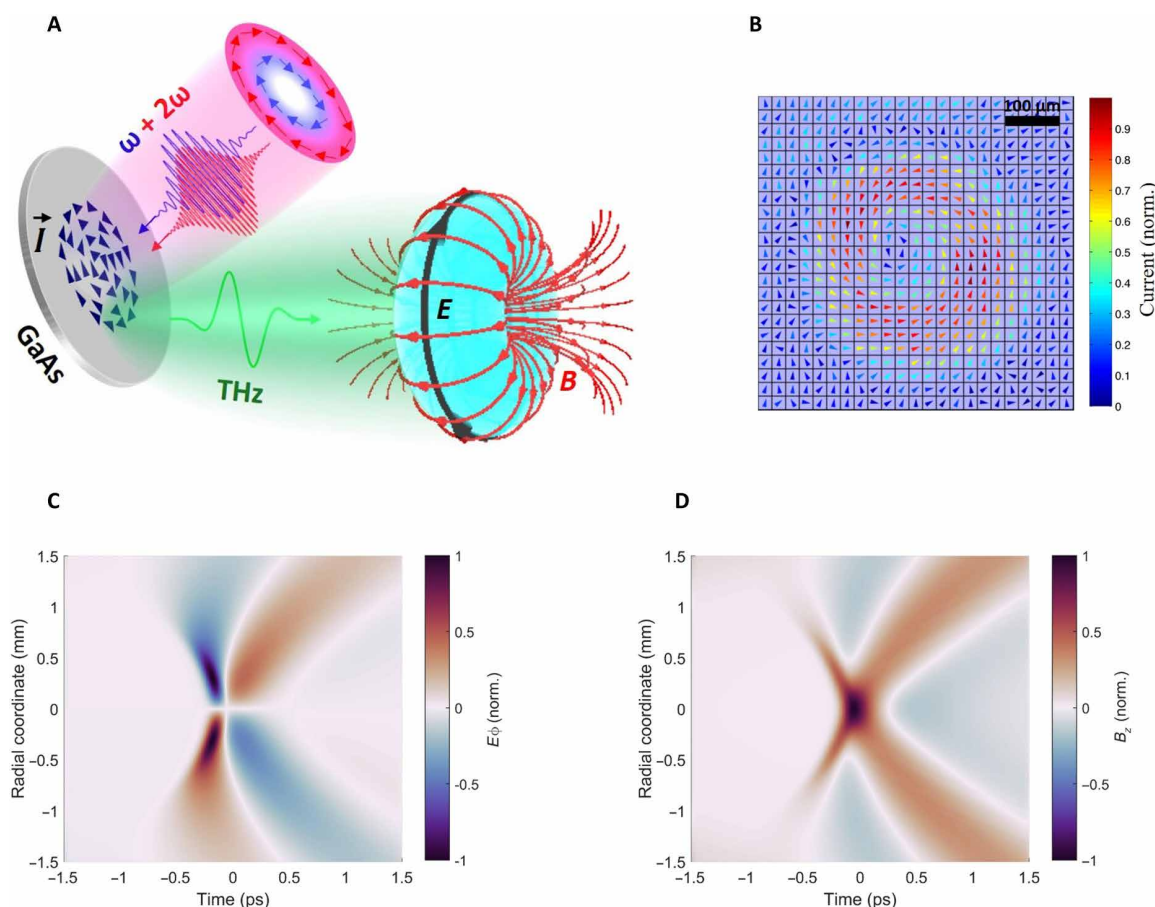
Fig. 1. Dynamic ring current radiates FD terahertz pulse. (**A**) Illustration of FD pulse generation. Two azimuthally polarized vector pulses generate transient ring currents in GaAs. The radiation from the rapidly oscillating ring currents is a single-cycle THz pulse with toroidal topology, an FD pulse. (**B**) Spatio-vectorial distribution of ring current measured with a single pixel current detector. Combining the detected *x* and *y* components (fig. S2) of the current results in spatial mapping of the ring current. (**C**) Spatiotemporal structure of the radiated electric field (E_φ) simulated using a dynamic ring current density source. (**D**) Simulated magnetic field (B_z) map of the emitted THz pulse.
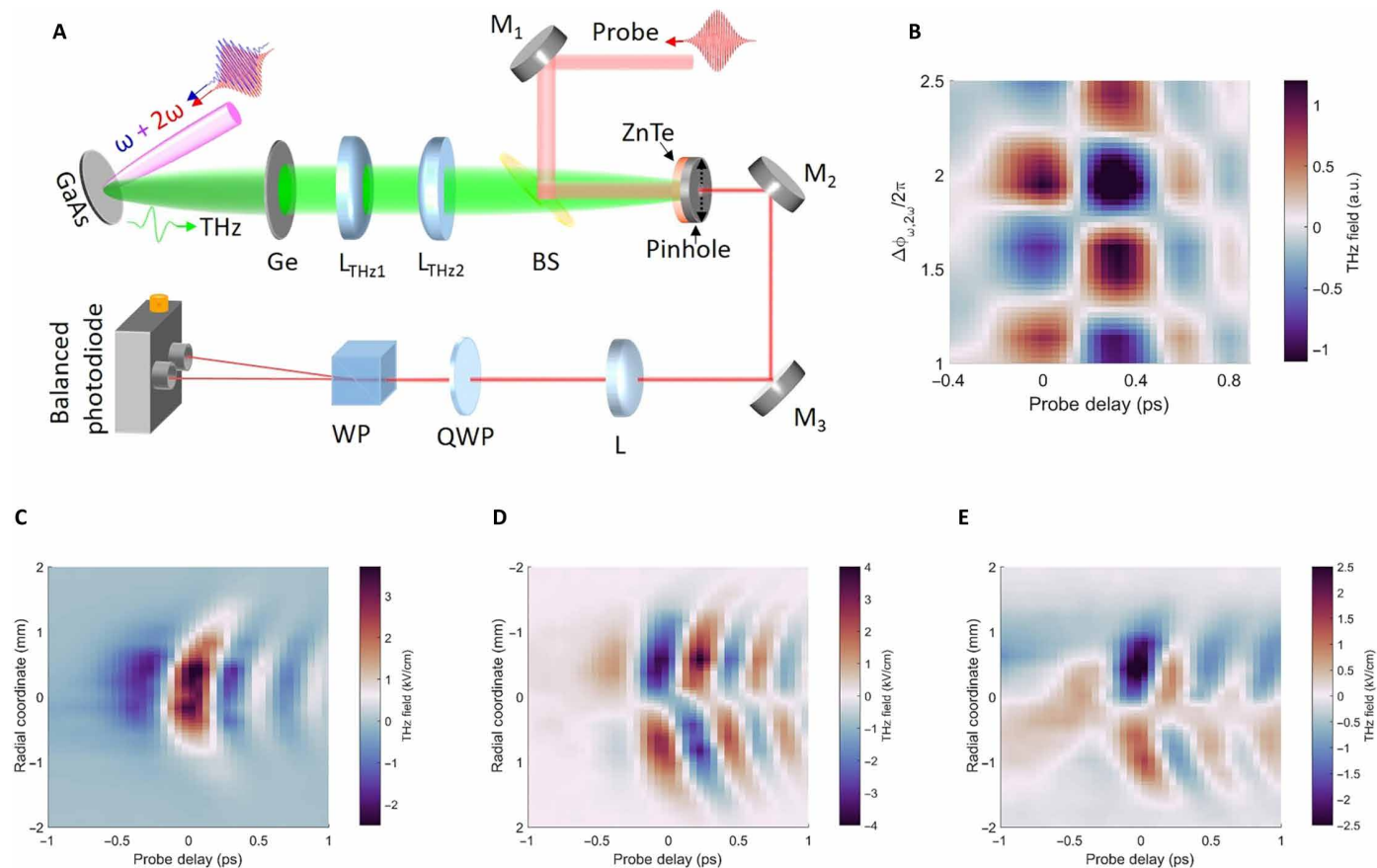
Fig. 2. Terahertz emission from two-color injected currents in GaAs. (**A**) Schematic of experimental setup for measuring terahertz radiation from transient currents excited in GaAs by synthesized two-color fields. GaAs, gallium arsenide substrate; Ge, germanium wafer; M_1 to M_3, metallic mirrors; L, focusing lens; L_{THz1} and L_{THz2}, THz lenses; QWP, quarter-wave plate; WP, Wollaston prism; BS, pellicle beam splitter; ZnTe, zinc telluride crystal. a.u., arbitrary units. (**B**) THz field as a function of two-color phase ($\Delta\varphi_{\omega,2\omega}$) and probe time delay. Terahertz waveforms are recorded at different values two-color phase. Spatiotemporal maps of the measured THz electric field when (**C**) linearly polarized (**D**) azimuthally polarized and (**E**) radially polarized two-color pulses are applied.

pulse arises from quantum control. Therefore, the amplitude and polarity of any structured single-cycle THz pulse generated in this manner can be controlled using the relative phase.

To spatially characterize the THz beam, we raster scan the probe beam with a 200-μm pinhole placed after the ZnTe crystal. The spatiotemporal profile of the THz pulse is obtained by recording the THz waveform at each position in the transverse plane of the beam. Figure 2C shows the measured spatiotemporal structure of the THz pulse emitted from the currents excited by linearly polarized Gaussian two-color laser pulses. Clearly, the measured THz beam also has a Gaussian spatial profile and exhibits a constant phase along the transverse direction, as expected from a unidirectional current source.

We then introduce q-plates (*21*) (orientation depicted in fig. S1B) to the experiment to produce two azimuthally (or radially) polarized vector pulses for quantum control of ring (or radial) currents in GaAs. The spatiotemporal profile of the THz pulse radiated from a ring current is measured and presented in Fig. 2D. We observe that the phase of the measured THz electric field is flipped along the radial direction and the field almost vanishes at the center. This corresponds to a doughnut-shaped structure as expected from the

calculation in Fig. 1C. Next, we change the polarization of the ω and 2ω light pulses from azimuthal to radial, which generates a radial current. In Fig. 2E, we present the measured space-time map of the radiated THz electric field from the radial current. The result shows similar phase singularity as seen with azimuthal polarization. Note that we can only measure the transverse components of the radially polarized mode as we use <110>-cut ZnTe crystal. For each of the spatiotemporal measurements, we observe that the electric field profiles are slightly asymmetric. The asymmetry is possibly due to inhomogeneous current generation in GaAs.

We also measure the spatial profiles $E_x(x, y)$ and $E_y(x, y)$ of the FD THz pulses (Fig. 3, A and B) radiated from the transient ring current. Spatial maps are measured at the peak of the THz waveform. The far-field spatial profiles closely resemble the two components of an azimuthally polarized beam. Similar measurements are also performed with radially polarized light pulses, which are presented in the Supplementary Materials (fig. S5). It shows that the positions and polarization of the radiated electric fields are interchanged with respect to those with azimuthal polarization. We see that, by simply changing the linear polarization direction of the Gaussian beam with which we start, we can interchange the roles of
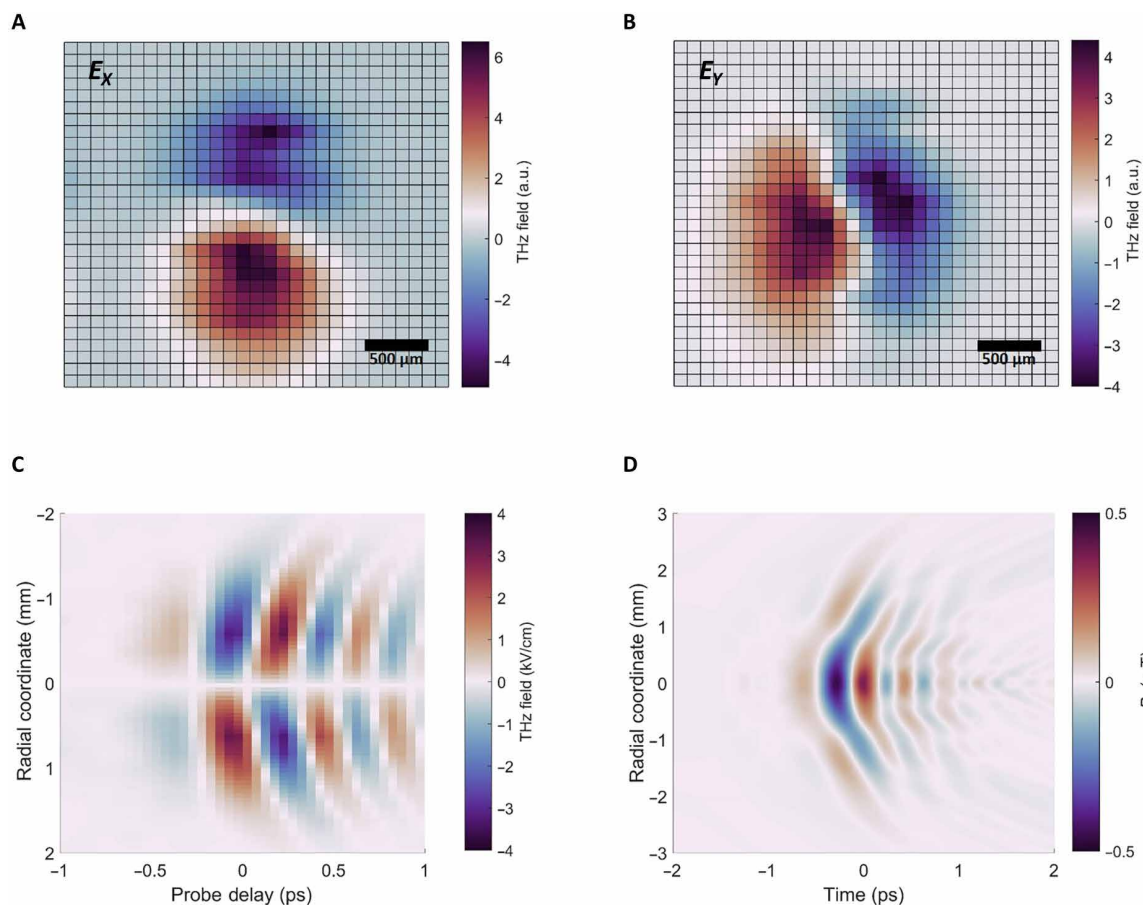
Fig. 3. Measurements of FD terahertz pulses. Far-field spatial maps of the FD THz pulse (**A**) $E_x (x, y)$ and (**B**) $E_y (x, y)$, radiated from ring current. Spatial profiles are measured at the peak of the THz waveform. (**C**) Spatiotemporal structure of electric field of the FD THz pulse. Measured data are symmetrized for magnetic field calculation. (**D**) Space-time structure of the calculated longitudinal magnetic field (B_z) of the FD pulse. The magnetic field is calculated from the measured electric field data using Maxwell's equations.

the electric and magnetic fields while still retaining the doughnut shape of the radiated pulse. Achieving such flexibility with metasurfaces is not trivial.

The measured spatiotemporal profile of the THz electric field enables us to calculate the space-time structure of the corresponding magnetic field using FDTD simulations. Performing these simulations in cylindrical coordinates means that we only require data from the positive or negative radial coordinates, i.e., half of the scan. The measured electric field structure is presented in Fig. 3C. The strength of the peak electric field is estimated to be 4 kV/cm. The calculated longitudinal magnetic field is presented in Fig. 3D, where the peak magnetic field strength is approximately 0.5 mT. Clearly, the position of the longitudinal magnetic field maximum coincides with the electric field singularity, making it suitable for sensitive control of spin and magnetic systems.

As a first application, we apply the FD THz pulse to THz time-domain spectroscopy (THz-TDS). Beyond being a very sensitive spectroscopic tool, THz-TDS enables us to obtain direct insight into how an absorption feature might influence the spatiotemporal structure of the emerging pulse, which may not be trivial. Here, we imprint a spectroscopic signature of water vapor onto the generated THz pulse by controlling the humidity level of the air through

which it propagates. We consider two situations: ambient air with a relative humidity (RH) of 41% (Fig. 4) and dry air with an RH of 12% (fig. S6). For the case of ambient air, we clearly observe oscillations after the main peak in the spatiotemporal structure of the measured THz electric field (Fig. 4A) due to absorption lines of water vapor (Fig. 4B). Figure 4C presents a calculated magnetic field map, where similar oscillatory features are clearly evident. Such absorption lines are also observed in the calculated magnetic field spectral profile (Fig. 4D).

From the measurement, we observe absorption features are mapped onto the measured electric and calculated magnetic field profiles. As expected, these linear, isotropic absorption features do not alter the spatial mode of the FD pulse. By applying the FD pulse and measurement technique to more complicated light-matter interaction involving nonlinear absorption or subwavelength structures, we would expect to see features of the light-matter interaction mapped onto the spatial mode of the pulse. By measuring the change in the spatial structure of the pulse, the nonlinear interaction can be diagnosed. Here, we use a space-time–coupled toroidal topological pulse that allows us to do high-temporal resolution spectroscopy of materials in response to either electric or magnetic fields. We also envisage that spatiotemporal THz modes such as the ones that we
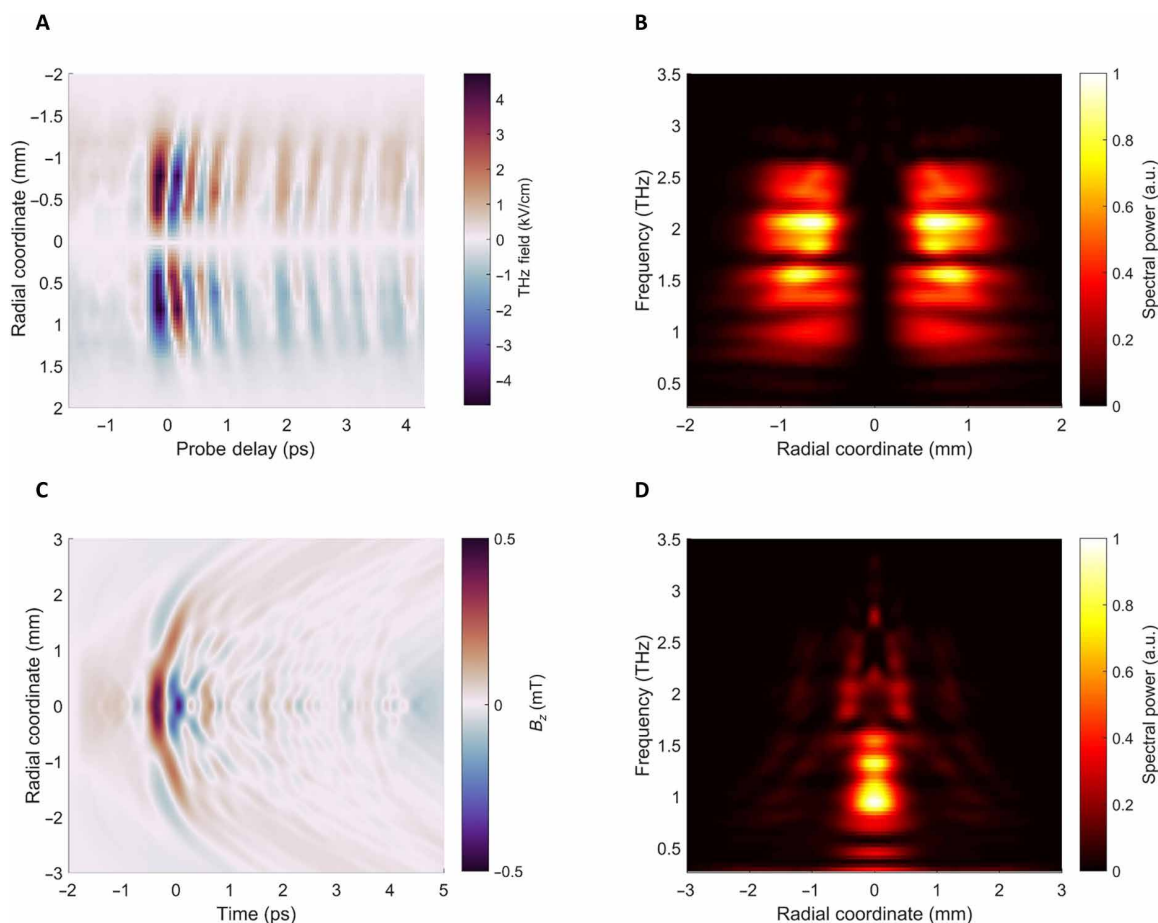
Fig. 4. Spectroscopy using FD pulse. (**A**) Measured electric field of FD pulses in humid air (RH 41%) condition. (**B**) Space-frequency representation of the measured electric field. (**C**) Calculated magnetic field (B_z) structure of the FD pulse in humid air. (**D**) Spatio-spectral map of the magnetic field B_z.

have demonstrated will be highly beneficial for spatially resolved THz spectroscopy and spectroscopy of toroidal systems (*22–24*).

DISCUSSION
In conclusion, we have demonstrated a new approach to metaoptics that eliminates the need for a structured material; instead, we generate transient current structures. Following this approach, we will be able to use tailored two-color laser fields to excite a single-cycle THz pulse with any mode, which is consistent with the material response and with Maxwell's equations. Similar active metastructures can also be generated and controlled in a gas medium (*25*), a multiphoton extension of what has been demonstrated here in a semiconductor. High intensity infrared structured light beams can be applied to gases to drive large current densities and yield high power THz radiation (*25–27*).

Using this approach, we have created a long–sought-after, far-field, spatiotemporal mode of light often called an FD in the THz domain. A substantial longitudinal magnetic field transient is present in the generated light mode. Such spatially isolated magnetic impulses are easily synchronized with ultrafast optical excitation and characterization schemes, and they are important for diagnosing the dynamic response of matter (*28–30*). We should mention that

these magnetic fields are too weak, as yet, to compete with an accelerator (*31*).

However, we should distinguish between near and far fields. Ours is a far-field measurement in which the collection efficiency of the optical system has not been fully optimized. Taking the collection and imaging efficiency of our optical system into account, we estimate that the peak magnetic field generated in GaAs would be approximately 10 mT or roughly 20 times greater than the measured value of 0.5 mT. We note that radiated field can be increased further by irradiating a larger area of the GaAs. In addition, using a nanostructured material, the THz magnetic field can be enhanced significantly (Supplementary Text S3). It is important to mention here that much larger magnetic fields are available in the near field, as presented in gas breakdown simulations (*25*). In the GaAs experiment presented here, the emission per unit area is limited by the need for the THz radiation created within the GaAs to escape through the over-dense plasma. This limit can be overcome by the much more energetic electrons created in gases (*25*) or in multilayer graphene (*32, 33*).

We have exploited the space-time–coupled structure of the FD pulse for a spectroscopic measurement of the distributed water vapor in ambient air. In this demonstration experiment, we observe that the absorption signature is mapped onto the space-time

structure of the measured electric field and calculated magnetic field profiles. Here, we do not observe any change in the spatial structure of the doughnut pulse due to the absorption. We expect that, for a nonlinear interaction, the interaction process will be diagnosed by measuring the change in spatial structure of the doughnut pulse. This is a characteristic of FD pulses, and it can be used for high–temporal resolution spectroscopy of materials in response to either electric or magnetic fields.

Last, while single-cycle light pulses have been available at THz frequencies for decades, it is only recently that technology has advanced sufficiently to produce single-cycle pulses in the visible and near infrared. This laser technology can almost certainly be extended to the mid-infrared (MIR) (34), where the CO_2 is an important gain medium. CO_2 lasers are polarization insensitive. Therefore, an azimuthally polarized pulse can be generated at low energy and then amplified to Joule-level picosecond pulses (35–37). Hollow-core fiber technology can already produce near single-cycle azimuthally or radially polarized pulses at 800 nm and this can almost certainly be scaled to Joule-level pulses in the MIR (35–39). Thus, we expect that CO_2 laser technology will give rise to high-power FD pulses with frequencies of ~30 THz and isolated magnetic fields that could approach amplitudes of 10^5 tesla with a wavelength-scale focal spot. An isolated 10^5 tesla and greater fields are only available from astronomical objects such as neutron stars (10^7 to 10^9 Tesla) or magnetic white dwarfs (10^2 to 10^5 tesla). Fields (10^5 tesla) are important because 10^5 tesla is approximately the field at which the atomic unit of energy (the energy that characterizes atomic hydrogen) equals the energy of an electron undergoing cyclotron motion i.e., $\hbar\omega = \hbar qB/m$, where q and m are the electron charge and mass, while B is the magnetic field strength (40). Even spectroscopy involving the ground state of the hydrogen atom is severely modified. For energies of this scale, 30 THz is essentially a static field.

MATERIALS AND METHODS
Optical system
The schematic of the full experimental setup is shown in fig. S1. The main fundamental beam centered at 1480 nm is obtained from a commercial optical parametric amplifier (TOPAS, Light Conversion) pumped by amplified 5-mJ, 800-nm femtosecond pulses (Legend Elite Duo, Coherent) operating at 1-kHz repetition rate. The fundamental beam is spatially filtered by passing it through a hollow core fiber kept in ambient air. The spatially filtered pulse is then transmitted through a beta-barium-borate crystal for second harmonic (740 nm) generation. Subsequently, a dichroic mirror is used to separate the two pulses. The two pulses of different wavelengths are independently manipulated in each arm of the interferometer. Their energy is controlled by a combination of a half wave plate and a polarizer. A liquid crystal wave plate (q-plate) is used to generate azimuthal polarization from the linearly polarized beam. After combining the two beams with a dichroic mirror, they propagate collinearly. Last, a lens is used to focus the two pulses onto the GaAs substrate to excite transient ring currents. The intensities of the fundamental (ω) and second harmonic (2ω) beams were kept at approximately 2×10^{11} W/cm^2 and 4×10^9 W/cm^2, respectively. A flip mirror mount is used to direct the bichromatic beam to either a current measurement or THz generation. A small part of the 2ω beam is used as the probe pulse for EOS of the terahertz waveforms. Using a pellicle beam splitter, the unfocused probe beam was aligned collinearly with the THz beam.

Simulations
The EOS measurements provide the space-time structure of a single slice of the THz pulse. We perform FDTD simulations to obtain the space-time structure of the complementary magnetic fields, along with an estimation of their amplitude. The FDTD code is homebuilt and is implemented in cylindrical coordinates. We assume that the fields are independent of the azimuthal coordinate, which reduces the simulation space to two dimensions. We use a uniform grid with $\Delta r = \Delta z = 5$ μm and $\Delta t = 11.7$ fs. The raw measured electric fields are used as a source in the simulations, and the three field components (E_φ, B_r, and B_z) are recorded after the pulse has propagated 4 mm.

Supplementary Materials
This PDF file includes:
Supplementary Text S1 to S3
Figs. S1 to S6
References

REFERENCES AND NOTES

1. H. Rubinsztein-Dunlop, A. Forbes, M. V. Berry, M. R. Dennis, D. L. Andrews, M. Mansuripur, C. Denz, C. Alpmann, P. Banzer, T. Bauer, E. Karimi, L. Marrucci, M. Padgett, M. Ritsch-Marte, N. M. Litchinitser, N. P. Bigelow, C. Rosales-Guzmán, A. Belmonte, J. P. Torres, T. W. Neely, M. Baker, R. Gordon, A. B. Stilgoe, J. Romero, A. G. White, R. Fickler, A. E. Willner, G. Xie, B. McMorran, A. M. Weiner, Roadmap on structured light. *J. Opt.* **19**, 013001 (2016).

2. A. Forbes, Structured light: Tailored for purpose. *Opt. Photonics News* **31**, 24–31 (2020).

3. L. Lu, J. D. Joannopoulos, M. Soljačić, Topological photonics. *Nat. Photonics* **8**, 821–829 (2014).

4. T. Pu, J.-Y. Ou, V. Savinov, G. Yuan, N. Papasimakis, N. I. Zheludev, Unlabeled far-field deeply subwavelength topological microscopy (DSTM). *Adv. Sci.* **8**, 20022886 (2020).

5. Y. Dai, Z. Zhou, A. Ghosh, R. S. K. Mong, A. Kubo, C. B. Huang, H. Petek, Plasmonic topological quasiparticle on the nanometre and femtosecond scales. *Nature* **588**, 616–619 (2020).

6. Z. Zhang, X. Qiao, B. Midya, K. Liu, J. Sun, T. Wu, W. Liu, R. Agarwal, J. M. Jornet, S. Longhi, N. M. Litchinitser, L. Feng, Tunable topological charge vortex microlaser. *Science* **368**, 760–763 (2020).

7. R. W. Hellwarth, P. Nouchi, Focused one-cycle electromagnetic pulses. *Phys. Rev. E* **54**, 889–895 (1996).

8. A. Zdagkas, C. McDonnell, J. Deng, Y. Shen, G. Li, T. Ellenbogen, N. Papasimakis, N. I. Zheludev, Observation of toroidal pulses of light. *Nat. Photonics* **16**, 523–528 (2022).

9. N. Papasimakis, T. Raybould, V. A. Fedotov, D. P. Tsai, I. Youngs, N. I. Zheludev, Pulse generation scheme for flying electromagnetic doughnuts. *Phys. Rev. B* **97**, 201409 (2018).

10. M. Koch, D. M. Mittleman, J. Ornik, E. Castro-Camus, Terahertz time-domain spectroscopy. *Nat. Rev. Methods Primers* **3**, 48 (2023).

11. S. Keren-Zur, M. Tal, S. Fleischer, D. M. Mittleman, T. Ellenbogen, Generation of spatiotemporally tailored terahertz wavepackets by nonlinear metasurfaces. *Nat. Commun.* **10**, 1778 (2019).

12. L. Luo, I. Chatzakis, J. Wang, F. B. P. Niesler, M. Wegener, T. Koschny, C. M. Soukoulis, Broadband terahertz generation from metamaterials. *Nat. Commun.* **5**, 3055 (2014).

13. X. C. Zhang, D. H. Auston, Optically induced THz electromagnetic radiation from planar photoconducting structures. *J. Electromagn. Waves Appl.* **6**, 85–106 (1992).

14. E. Dupont, P. B. Corkum, H. C. Liu, M. Buchanan, Z. R. Wasilewksi, Phase-controlled currents in semiconductors. *Phys. Rev. Lett.* **74**, 3596–3599 (1995).

15. R. Atanasov, A. Haché, J. L. P. Hughes, H. M. van Driel, J. E. Sipe, Coherent control of photocurrent Generation in bulk semiconductors. *Phys. Rev. Lett.* **76**, 1703–1706 (1996).

16. M. Shapiro, P. Brumer, *Quantum Control of Molecular Processes* (John Wiley & Sons, 2011).

17. S. Sederberg, F. Kong, F. Hufnagel, C. Zhang, E. Karimi, P. B. Corkum, Vectorized optoelectronic control and metrology in a semiconductor. *Nat. Photonics* **14**, 680–685 (2020).

18. K. Jana, K. R. Herperger, F. Kong, Y. Mi, C. Zhang, P. B. Corkum, S. Sederberg, Reconfigurable electronic circuits for magnetic fields controlled by structured light. *Nat. Photonics* **15**, 622–626 (2021).

19. K. Jana, E. Okocha, S. H. Møller, Y. Mi, S. Sederberg, P. B. Corkum, Reconfigurable terahertz metasurfaces coherently controlled by wavelength-scale-structured light. *Nanophotonics* **11**, 787–795 (2022).

20. S. Sederberg, P. B. Corkum, Perspective on phase-controlled currents in semiconductors driven by structured light. *Appl. Phys. Lett.* **120**, 160504 (2022).

21. H. Larocque, J. Gagnon-Bischoff, F. Bouchard, R. Fickler, J. Upham, R. W. Boyd, E. Karimi, Arbitrary optical wavefront shaping via spin-to-orbit coupling. *J. Opt.* **18**, 124002 (2016).

22. N. I. Zheludev, D. Wilkowski, The rise of toroidal electrodynamics and spectroscopy. *ACS Photonics* **10**, 556–558 (2023).

23. I. Kuprov, D. Wilkowski, N. Zheludev, Toroidal optical transitions in hydrogen-like atoms. *Sci. Adv.* **8**, eabq6751 (2022).

24. T. A. Raybould, V. A. Fedotov, N. Papasimakis, I. Kuprov, I. J. Youngs, W. T. Chen, D. P. Tsai, N. I. Zheludev, Toroidal circular dichroism. *Phys. Rev. B* **94**, 035119 (2016).

25. S. Sederberg, F. Kong, P. B. Corkum, Tesla-scale terahertz magnetic impulses. *Phys. Rev. X* **10**, 011063 (2020).

26. S. Wang, Y. Bai, P. Liu, Generation of terahertz spatiotemporal optical vortices with frequency-dependent orbital angular momentum. *Opt. Express* **31**, 16267–16280 (2023).

27. Y. Mi, K. Johnston, V. Shumakova, S. H. Møller, K. Jana, C. Zhang, A. Staudte, S. Sederberg, P. B. Corkum, Active stabilization of terahertz waveforms radiated from a two-color air plasma. *Photonics Res.* **10**, 96–103 (2022).

28. A. Kirilyuk, A. V. Kimel, T. Rasing, Ultrafast optical manipulation of magnetic order. *Rev. Mod. Phys.* **82**, 2731–2784 (2010).

29. K. Yamaguchi, M. Nakajima, T. Suemoto, Coherent control of spin precession motion with impulsive magnetic fields of half-cycle terahertz radiation. *Phys. Rev. Lett.* **105**, 237201 (2010).

30. K. Yamaguchi, T. Kurihara, Y. Minami, M. Nakajima, T. Suemoto, Terahertz time-domain observation of spin reorientation in orthoferrite ErFeO3 through magnetic free induction decay. *Phys. Rev. Lett.* **110**, 137204 (2013).

31. I. Tudosa, C. Stamm, A. B. Kashuba, F. King, H. C. Siegmann, J. Stöhr, G. Ju, B. Lu, D. Weller, The ultimate speed of magnetic switching in granular recording media. *Nature* **428**, 831–833 (2004).

32. T. Higuchi, C. Heide, K. Ullmann, H. B. Weber, P. Hommelhoff, Light-field-driven currents in graphene. *Nature* **550**, 224–228 (2017).

33. D. Sun, C. Divin, J. Rioux, J. E. Sipe, C. Berger, W. A. Heer, P. N. First, T. B. Norris, Coherent control of ballistic photocurrents in multilayer epitaxial graphene using quantum interference. *Nano Lett.* **10**, 1293–1296 (2010).

34. F. Kong, H. Larocque, E. Karimi, P. B. Corkum, C. Zhang, Generating few-cycle radially polarized pulses. *Optica* **6**, 160–164 (2019).

35. D. Haberberger, S. Tochitsky, C. Joshi, Fifteen terawatt picosecond CO_2 laser system. *Opt. Express* **18**, 17865–17875 (2010).

36. M. N. Polyanskiy, I. V. Pogorelsky, M. Babzien, R. Kupfer, K. L. Vodopyanov, M. A. Palmer, Post-compression of long-wave infrared 2 picosecond sub-terawatt pulses in bulk materials. *Opt. Express* **29**, 31714–31725 (2021).

37. P. B. Corkum, Amplification of picosecond 10 μm pulses in multiatmosphere CO2 lasers. *IEEE J. Quantum Electron.* **21**, 216–232 (1985).

38. M. N. Polyanskiy, I. V. Pogorelsky, M. Babzien, R. Kupfer, N. Vafaei-Najafabadi, M. A. Palmer, High-peak-power long-wave infrared lasers with CO_2 amplifiers. *Photonics* **8**, 101 (2021).

39. S. Carbajo, E. Granados, D. Schimpf, A. Sell, K. H. Hong, J. Moses, F. X. Kärtner, Efficient generation of ultra-intense few-cycle radially polarized laser pulses. *Opt. Lett.* **39**, 2487–2490 (2014).

40. P. Schmelcher, L. S. Cederbaum, in *High Magnetic Fields: Science and Technology*, vol. 2, F. Herlach, N. Miura, Eds. (World Scientific, 2003), pp. 245–266.

41. M. C. Hoffmann, S. Schulz, S. Wesch, S. Wunderlich, A. Cavalleri, B. Schmidt, Coherent single-cycle pulses with MV/cm field strengths from a relativistic transition radiation light source. *Opt. Lett.* **36**, 4473–4475 (2011).

42. D. Côté, J. M. Fraser, M. DeCamp, P. H. Bucksbaum, H. M. van Driel, THz emission from coherently controlled photocurrents in GaAs. *Appl. Phys. Lett.* **75**, 3959–3961 (1999).

43. M. Blanco, F. Cambronero, M. T. Flores-Arias, E. C. Jarque, L. Plaja, C. Hernández-Garcíaet, Ultraintense femtosecond magnetic nanoprobes induced by azimuthally polarized laser beams. *ACS Photonics* **6**, 38–42 (2019).

44. D. Polley, N. Z. Hagström, C. von Kroff Schmising, S. Eisebitt, S. Bonetti, Terahertz magnetic field enhancement in an asymmetric spiral metamaterial. *J. Phys. B At. Mol. Opt. Phys.* **51**, 224001 (2018).

45. J. A. Riordan, F. G. Sun, Z. G. Lu, X.-C. Zhang, Free-space transient magneto-optic sampling. *Appl. Phys. Lett.* **71**, 1452–1454 (1997).

Science Advances

Quantum control of flying doughnut terahertz pulses

Kamalesh Jana, Yonghao Mi, Søren H. Møller, Dong Hyuk Ko, Shima Gholam-Mirzaei, Daryoush Abdollahpour, Shawn Sederberg, and Paul B. Corkum

View the article online
https://www.science.org/doi/10.1126/sciadv.adl1803
Permissions
https://www.science.org/help/reprints-and-permissions

Use of this article is subject to the Terms of service